European Polymer Journal 139 (2020) 109989

Contents lists available at ScienceDirect

European Polymer Journal

journal homepage: www.elsevier.com/locate/europolj

Confined crystallization and degradation of six-arm star PCL with core of cyclotriphosphazene in epoxy thermosets

Pengli Zhang, Yanfang Zhao, Rentong Yu*, Jianhe Liao*

School of Materials Science and Engineering, Hainan University, Haikou 570228, PR China

ARTICLE INFO

Keywords:
Confined crystallization
Epoxy thermosets
Six-arm star PCL with core of cyclotriphosphazene
Degradation

ABSTRACT

Six-arm star polycaprolactone with core of cyclotriphosphazene (*s*-PCL) was synthesized via ring-opening polymerization and characterized by NMR and GPC. Epoxy thermosets incorporating 10–40 *wt*% of this copolymer were cured with 4,4′-methylenebis(2-chloroaniline) (MOCA) and 4,4′-diaminodiphenyl sulfone (DDS), respectively. In these thermosets, intermolecular specific interactions had a significant impact on their morphologies. Specifically, no discernable macroscopic phase separation was found in FESEM images of MOCA-cured epoxy resins. However, for the DDS-cured system, *s*-PCL was partially miscible with the epoxy thermosets, as evidenced with FTIR and DMA. This is may be owning to enriched concentration of hydroxyl groups in the *s*-PCL favored the miscibility between PCL subchains of carbonyl and the epoxy matrix. Dispersed phase, further confirmed by XRD to be amorphous, with a diameter of 0.34–0.44 μm could be observed (*s*-PCL' content ≤ 20 *wt* %) in this system. Nevertheless, crystallization of PCL could not be suppressed completely (*s*-PCL' content > 30 *wt*%). Besides, epoxy thermosets containing crystalline PCL were found to be more resistant to thermal degradation but sensitive to alkaline degradation (10% NaOH aqueous solution) according to TGA and FESEM results. This work presented here is a meaningful report on the presence of alkaline-labile crosslinking points through the whole networks.

1. Introduction

In the past decades, numerous amphiphilic block copolymers and hybrid copolymers have been synthesized and utilized as modifiers for bisphenol A diglycidyl ether (DGEBA) type epoxy resin, a typical and commonly used thermoset. Based on exquisite molecular design of copolymers, epoxy thermosets affected by reaction induced micro-phase separation or self-assembly mechanism could be achieved with various kinds of morphologies such as spherical, bicontinuous, hexagonal as well as lamellar phases, endowing them with excellent properties [1–4]. By tailoring the microstructure of these thermosets, their mechanical properties can be improved notably. Fracture toughness of these materials, for example, can be enhanced by nanostructured morphologies of wormlike micelles, vesicles, etc. [5]. Epoxy thermosets can also be functionalized on account of characteristics of their subchains. The charge transfer complexes formed between poly(ethylene oxide)-*b*-poly (N-vinylcarbazole) and fullerene-capped poly(ethylene oxide) reduced the dielectric constant of epoxy matrix [6]. Besides, epoxy thermosets with well-organized structure could serve as templates for peculiar purposes. For instance, nanoporous epoxy resin with high protein adsorbability can be obtained via self-assembly of diblock copolymer [7]. Modulating the morphology of epoxy thermosets has been proved to be pivotal for their wide applications.

Polycaprolactone (PCL), a semicrystalline and biodegradable polymer, has often been employed in blending with epoxy resin [8–10]. PCL is a suitable additive which is miscible with epoxy matrix cured with certain amine-type curing agents, such as 4,4′-methylene bis(2-chloroaniline) (MOCA), due to intermolecular interactions (hydrogen bonding) in cured systems [11]. Particularly, diverse amphiphilic copolymers and hybrid copolymers containing PCL can be incorporated into epoxy thermosets, which may have a critical influence on the behavior of phase separation behavior in epoxy matrix [12,13]. However, it is commonly recognized that amine-type curing agents are not bound to facilitate the miscibility between PCL and epoxy matrix [14,15]. For DDS-cured blends, the formation of hydrogen bonding between secondary hydroxyl groups in the epoxy crosslinks and the carbonyl groups of linear-PCL is suppressed due to the existence of OH···S=O hydrogen bonding interactions [11]. Hereby, whether the miscibility of DDS-cured epoxy resin/PCL blends can be improved in case that the per unit volume concentration of hydroxyl groups of PCL could be increased? In this case, multi-armed PCL could be miscible with DDS-cured epoxy matrix. In other words, enriched proportion of carbonyl groups accompanying conformation motion of PCL subchains may exercise influence on the competitive hydrogen bonding interactions and then

* Corresponding authors.

https://doi.org/10.1016/j.eurpolymj.2020.109989
Received 29 June 2020; Received in revised form 26 August 2020; Accepted 29 August 2020
Available online 07 September 2020

facilitate the miscibility between PCL and epoxy matrix. Moreover, the change in miscibility may affect crystallization behavior of PCL. It is normally accepted that linear PCL crystallizes well in epoxy thermosets cured with DDS, although chain folding and crystallization of PCL would be suppressed by the crosslinking structure of epoxy matrix [16,17]. Apparently, the crystallization of linear PCL is confined in a three-dimensional network in this case. It is reasonable to speculate that degradation of epoxy thermosets containing PCL would be affected by the condensed structure of PCL, amorphous or crystalline.

In this work, six-arm star polycaprolactone with core of cyclotriphosphazene (*s*-PCL) was synthesized, introduced to epoxy resin, and then cured with MOCA and DDS, respectively. The miscibility between PCL subchains and epoxy matrix was investigated by means of FTIR and DMA. The morphologies of the blends were characterized by FESEM and XRD analyses. The relationship between confined crystallization of the subchains of *s*-PCL and miscibility of the compounds was also evaluated. Furthermore, thermal degradation and alkaline hydrolysis of the two amine-type cured thermosets were investigated.

2. Material and methods

2.1. Materials

Sodium borohydride 4,4′-diaminodiphenyl sulfone and solvents including tetrahydrofuran, *n*-hexane and toluene were supplied by Shanghai Reagent Co, China. Prior to use, the solvents were dried by distillation over sodium. Hexachlorocyclotriphosphazene (HCCP), sodium hydride (60% dispersion in mineral oil), 4-hydroxybenzaldehyde, stannous (II) octanoate [$Sn(Oct)_2$], 4,4′-methylene-bis(2-chloroaniline) and anhydrous ethanol were purchased from J&K Scientific Reagent Co., China. HCCP was recrystallized twice from anhydrous hexane before use. Calcium hydride was supplied by Aladdin Reagent Co, China. ∈-Caprolactone was obtained from Sigma-Aldrich Reagent Co., dried over calcium hydride for one week and distilled under reduced pressure before use. Methanol and ethanol were purchased from Xilong Science Reagent Co, China. Bisphenol A diglycidyl ether (DGEBA), with epoxy equivalent weight of 185–210, was supported by Shanghai Resin Co., China. Deionized water was prepared in our laboratory.

2.2. Synthesis of the hexa-hydroxyl initiator

The *hexa*-hydroxyl initiator (HHMPCP) was synthesized according to Luo's work [18]. In a typical procedure, sodium hydride (1.8 g, 45 mmol) was dissolved in 50 mL of anhydrous tetrahydrofuran in a flask with stirring under nitrogen. A solution of 4-p-hydroxybenzaldehyde (5.5 g, 45 mmol) in 50 mL anhydrous tetrahydrofuran was then added into the above solution slowly. The reaction was carried out at room temperature for 4 h. Then, HCCP (1.7 g, 5 mmol), dissolved in 50 mL anhydrous tetrahydrofuran, was reacted with the aforementioned system and the reaction was performed at reflux temperature for 48 h. The mixture was suction filtered and then concentrated *via* rotary evaporation thrice. The crude product, (hexa[p-(aldehyde)phenoxy] cyclotriphosphazene, HAPCP), was recrystallized from ethyl acetate twice and dried under vacuum overnight (yield of HAPCP: 53%).

Next, HAPCP (0.8 g, 0.93 mmol) was dissolved in anhydrous tetrahydrofuran/methanol (50 mL, v/v = 1:1) and added into a flask. Then, sodium borohydride (0.27 g, 7.19 mmol) was mixed in the flask step by step with vigorous stirring in ice-water bath. After that, the reaction was allowed to proceed at room temperature for 14 h. The reaction mixture was concentrated by rotary evaporation. Before filtration under vacuum, the crude initiator (hexa[p-(hydroxymethyl) phenoxy] cyclotriphosphazene, HHMPCP) was washed with deionized water 3 times. The mixture was recrystallized with ethanol, and then dried under vacuum overnight (yield of HHMPCP: 67%).

HAPCP: ^{1}H NMR ($CDCl_3$, ppm): 9.93 (6H, C**H**O), 7.72, 7.15 (24H, $C_6\mathbf{H}_4$)

HHMPCP: ^{1}H NMR (DMSO-d_6, ppm): 7.18, 6.78 (24H, $C_6\mathbf{H}_4$), 5.22 (6H, O**H**), 4.43 (12H, $C\mathbf{H}_2$).

2.3. Synthesis of six-arm star polycaprolactone with cyclotriphosphazene core

In the presence of the *hexa*-hydroxyl initiator, ∈-caprolactone was adopted as monomer with stannous (II) octanoate as the catalyst to synthesize *s*-PCL by ring opening polymerization (ROP)[18]. Typically, HHMPCP (0.304 g, 0.3 mmol), ∈-caprolactone (10.564 g, 92.6 mmol) and stannous (II) octanoate (2 *wt*‰ of ∈-caprolactone) were mixed in a flask with a magnetic agitator. The flask was installed to a Schlenk system to degas oxygen completely. The polymerization was performed under nitrogen at 110 °C for 48 h. The reaction product was precipitated into cold petroleum ether. After filtration in *vacuo*, the residues were dried under vacuum overnight (yield of *s*-PCL: 96.2%).

s-PCL: ^{1}H NMR ($CDCl_3$, ppm): 4.06 (2H, HO**CH2**CH2CH2CH2CH2OCO), 2.31 (2H, −OCO**CH2**), 1.65 (4H, OCOCH2**CH2**CH2**CH2**CH2), 1.39 (2H, OCOCH2CH2**CH2**CH2CH2).

2.4. Preparation of epoxy thermosets

Planned amounts of *s*-PCL and DGEBA, and a stoichiometric amount of DDS vis-a-vis DGEBA were blended. The MOCA curing system was prepared in the same way. The mixtures were vigorously stirred at 150 °C (for DDS-cured system) and 100 °C (for MOCA-cured system) until they became transparent and homogenous. The systems were cured at 150 °C for 3 h and then post-cured at 180 °C for 2 h.

2.5. Measurements and techniques

Nuclear magnetic resonance spectra (^{1}H NMR and ^{31}P NMR) were conducted on a Bruker AV 400 NMR spectrometer at 400 MHz and 25 °C, using deuterated chloroform ($CDCl_3$) and dimethyl sulfoxide (DMSO-d_6) as solvents and tetramethylsilane (TMS) as the internal standard. Gel permeation chromatography (GPC) of *s*-PCL were obtained on a Waters 1515 system provided with Waters polystyrene columns and a Waters refractive index detector, whereas tetrahydrofuran was employed as the eluent at a rate of 1.0 mL/min. Fourier transform infrared spectra (FTIR) were made an acquisition on a PerkinElmer Spectrum One FTIR spectrometer. All samples were blended with KBr in the form of powder and then compressed into tablets. The spectra were collected with 16 scans and a resolution of 2 cm^{-1}. Thermal gravimetric analysis (TGA) was conducted on a TA Q600 thermogravimetric analyzer. The specimen was heated from 30 °C to 600 °C under nitrogen atmosphere at a rate of 10 °C/min. All the samples were dried in an 80 °C oven for 24 h prior to testing. Dynamic mechanical thermal analysis (DMA) was performed on a TA Q800 instrument. The materials were heated from 30 °C to 250 °C at a rate of 3.0 °C/min with the frequency of 1.0 Hz and in single cantilever mode. The specimen dimensions were $30 \times 10 \times 3$ mm^3. X-ray diffraction (XRD) characterization was carried out on a Brucker D 8 Advance diffractometer with Cu Kα radiation (λ = 1.542 Å). The specimen was scanned from 10° to 90°, with step size of 0.02 and scan speed of 6°/min. Field emission scanning electron microscopy (FESEM) was performed using a ZEISS SIGMA Field Emission SEM with an electron voltage of 10 kV. The samples were fractured in liquid nitrogen, dried in vacuum oven and coated with gold before scanning. The samples were immersed in 10% NaOH aqueous solution at 40 °C for degradation. After 30 days, the samples were taken out, washed with ethanol and sonicated. The materials were dried at 60 °C for 48 h before tests.

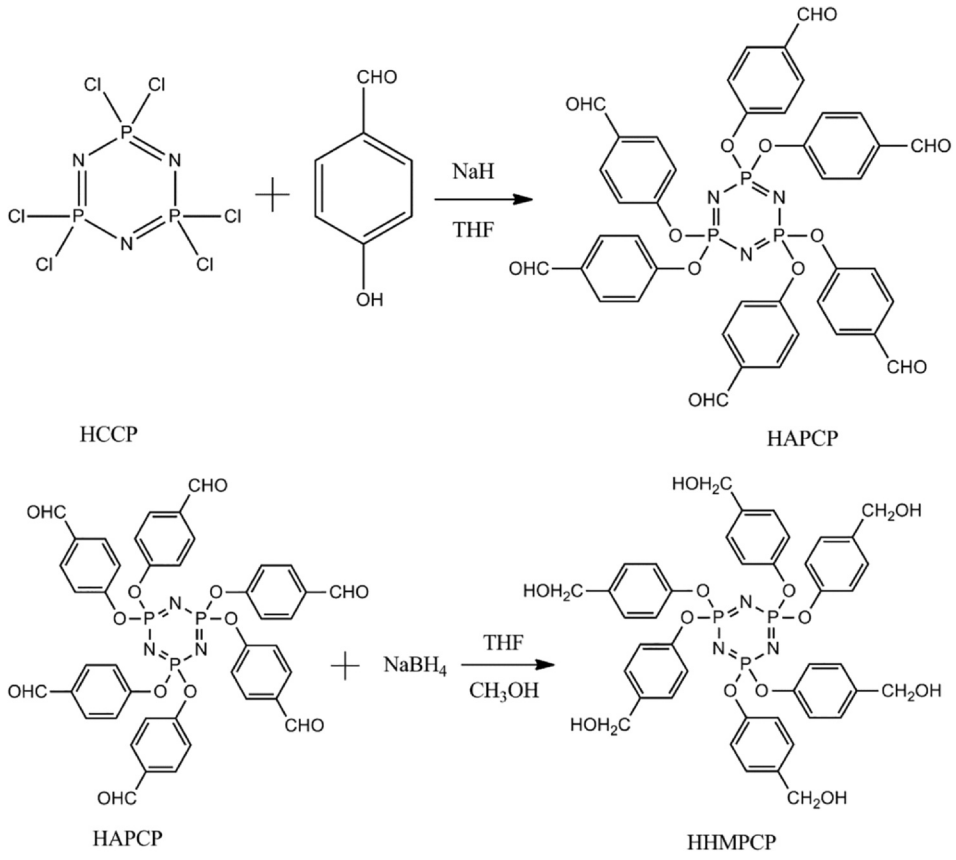

Scheme 1. Synthesis of the *hexa*-hydroxyl initiator (HHMPCP).

3. Results and discussion

3.1. Synthesis of the hexa-hydroxyl initiator

The synthetic procedure for the *hexa*-hydroxyl initiator (HHMPCP) is presented in Scheme 1. HAPCP was synthesized *via* a substitution reaction between 4-p-hydroxybenzaldehyde and HCCP. After all the –CHO groups of HAPCP were reduced to –OH groups with sodium borohydride, the *hexa*-hydroxyl initiator was obtained. The product was confirmed by the results of NMR (Fig. 1; Fig. S1) and FTIR (Fig. S2)

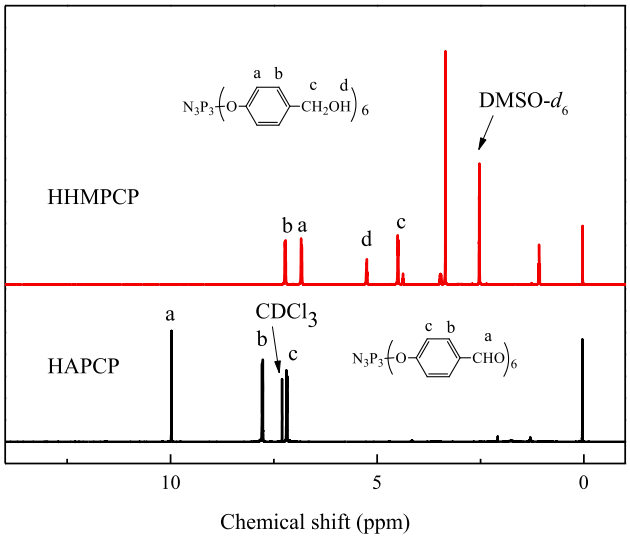

Fig. 1. ^{1}H NMR spectra of intermediate (HAPCP, the solvent was $CDCl_3$) and HHMPCP (the solvent was DMSO-d_6).

analyses. In the ^{1}H NMR spectrum of HAPCP shown in Fig. 1, the signal at 9.94 ppm was ascribed to the −CHO proton of HAPCP, and the weak peaks which appeared at chemical shifts of 7.74 ppm and 7.15 ppm were assigned to the protons from benzene ring. In the ^{1}H NMR spectrum of HHMPCP, the signal of the −CHO proton in HAPCP completely disappeared, and several new signals at 5.22 ppm and 4.47 ppm appeared, indicating the presence of −OH and $-CH_2$ groups of the initiator, respectively (Fig. 1). Therefore, the initiator was obtained successfully, which was also verified by FTIR (Fig. S2). The FTIR absorption peaks observed at 600 cm^{-1} and 520 cm^{-1} were due to the vibration band of −P−Cl− in HCCP. After the substitution reaction, a new band appeared at 1705 cm^{-1}, which was attributed to the stretching vibration of aromatic aldehyde −CHO of HAPCP. Besides, the new absorption peaks at 1598 cm^{-1} and 1501 cm^{-1} were assigned to aromatic skeleton vibration, suggesting that chlorine atoms of HCCP were substituted by 4-p-hydroxybenzaldehyde successfully. Compared with the spectrum of HAPCP, a broad band appeared at 3373 cm^{-1} in the spectrum of HHMPCP due to the stretching vibration of hydroxyl groups -O-H of HHMPCP.

3.2. Synthesis of six-arm star polycaprolactone with cyclotriphosphazene core

The synthetic route of six-arm PCL is depicted in Scheme 2. HHMPCP was used as the initiator for the ring-opening polymerization of *s*-PCL. Fig. 2 illustrates the ^{1}H NMR spectrum of *s*-PCL. Signals of resonance at 4.06 ppm, 3.65 ppm, 2.31 ppm, 1.65 ppm, and 1.39 ppm were assigned to the methylene protons ($-CH_2$) of PCL chains. Weak signals appeared at chemical shifts of 7.16 ppm and 6.92 ppm, which were due to the protons of benzene ring in *s*-PCL. The results were further confirmed by FTIR (Fig. S3). An absorption band at 1727 cm^{-1} was attributed to the stretching vibration of carbonyl −C═O. Fig. 3

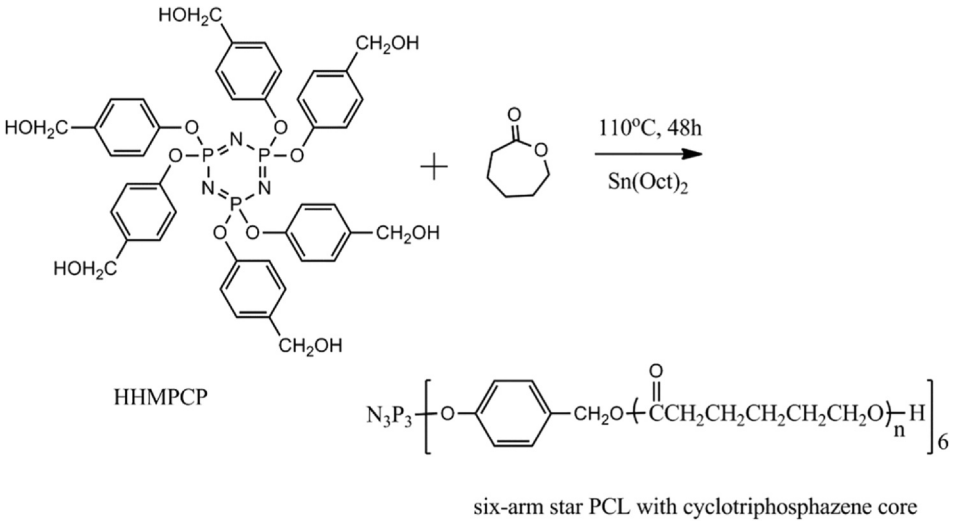

Scheme 2. Synthesis of six-arm star PCL with cyclotriphosphazene core (*s*-PCL).

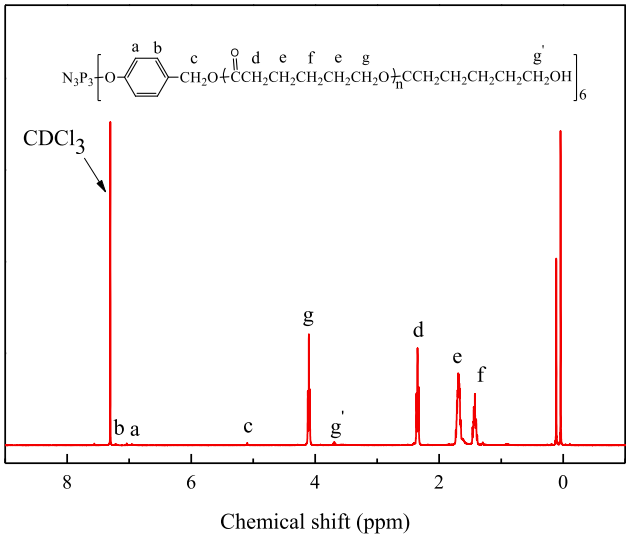

Fig. 2. ^{1}H NMR spectrum of *s*-PCL (the solvent was $CDCl_3$).

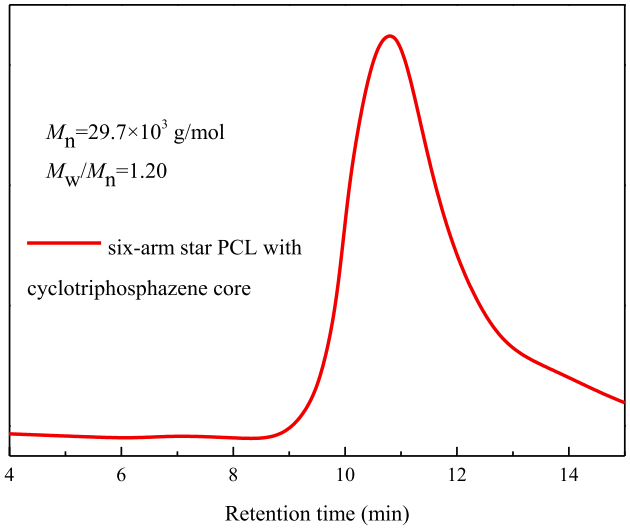

Fig. 3. GPC curve of *s*-PCL (the solvent was tetrahydrofuran).

shows the GPC curves and molecular weight information of *s*-PCL. The polydispersity index of *s*-PCL was 1.20, suggesting that the distribution of molecular weight was adequately narrow. From Fig. 3, the number averaged molecular weight of *s*-PCL was calculated to be 29.7 × 10^3 g/mol.

3.3. Preparation of epoxy thermosets containing six-arm PCL and intermolecular specific interactions between them

In this work, two amine-type curing agents, MOCA and DDS, were selected to cure the blends of DGEBA and *s*-PCL. Details of the curing systems are shown in Table 1. Prior to curing, *s*-PCL, DGEBA and the curing agents were transparent without any macroscopic phase separation. After curing, the cured products with MOCA were transparent, while the thermosets cured with DDS were opaque (Fig. S4). Fig. S5 presents the FTIR spectra of MOCA-cured and DDS-cured thermosets. In contrast to the cured system without PCL, the absorption peak of the carbonyl groups −C═O appeared at the wavenumber of 1727 cm^{-1} in epoxy thermosets containing PCL.

Additionally, in order to investigate the intermolecular specific interactions between carbonyl groups of *s*-PCL subchains and secondary hydroxyls of epoxy matrix cured with DDS, FTIR spectra with respect to carbonyl stretching vibration are shown in Fig. 4a with the region between 1660 cm^{-1} and 1800 cm^{-1}. Upon increasing the content of *s*-PCL, the absorption band of carbonyl stretching vibration shifted to low wavenumber. Hence, the existence of intermolecular specific interactions between PCL and epoxy matrix can be confirmed [11]. Moreover, a band appeared at 1727 cm^{-1} for the sample with 40 *wt*% of *s*-PCL, which is the characteristic evidence of carbonyl of crystalline PCL. Generally, bands at 1735 cm^{-1} and 1727 cm^{-1} can be assigned to

Table 1
Formulas and thermal degradation data of the epoxy thermosets.

Sample	Hardener	*s*-PCL	T_5 (°C)	Char yield (%)
M-1	MOCA	10 *wt*% *s*-PCL	334	28.7
M-2		20 *wt*% *s*-PCL	333	32.2
M-3		30 *wt*% *s*-PCL	329	29.4
M-4		40 *wt*% *s*-PCL	317	29.3
D-1	DDS	10 *wt*% *s*-PCL	349	31.2
D-2		20 *wt*% *s*-PCL	336	23.3
D-3		30 *wt*% *s*-PCL	261	21.0
D-4		40 *wt*% *s*-PCL	334	27.0

Bisphenol A diglycidyl ether (DGEBA) acts as the epoxy precursor. The values of char yield of samples were obtained at 600 °C.

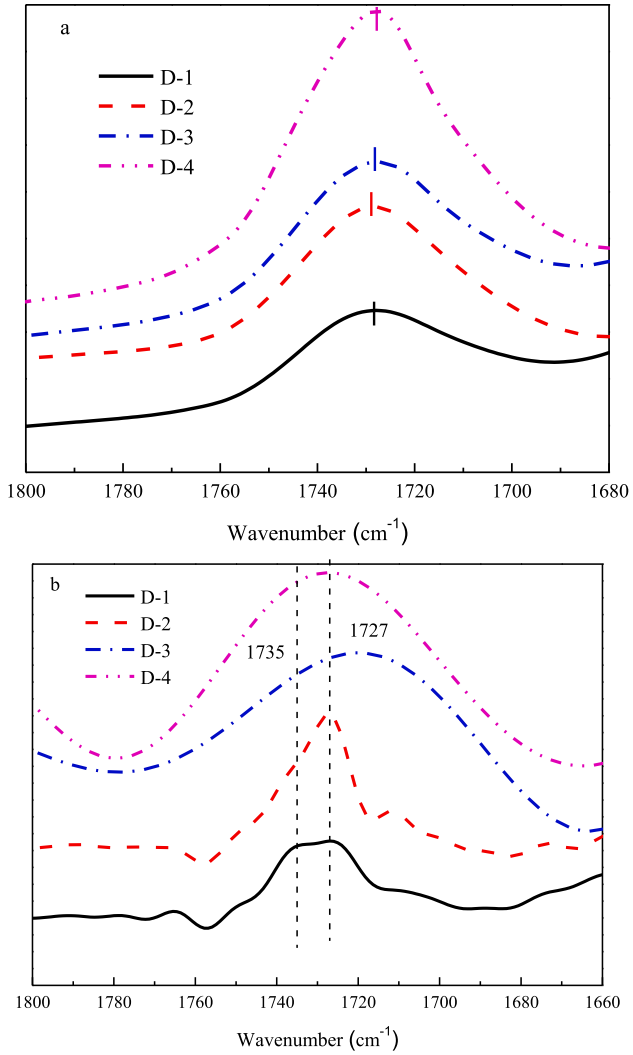

Fig. 4. FTIR spectra of DDS-cured epoxy thermosets containing *s*-PCL. (a) FTIR spectra in the range of 1660–1800 cm^{-1}. (b)FTIR spectra processing by fourier deconvolution method.

amorphous and crystalline states of PCL, respectively [11]. However, they could not be easily distinguished due to overlap. To overcome this, Fourier deconvolution method was used and the corresponding results are presented in Fig. 4b. With increase in the content of *s*-PCL, the intensity of the band centered at 1735 cm^{-1} became significantly weaker, suggesting that crystallization of the *s*-PCL subchains could not be suppressed completely. At the same time, the carbonyl band indicated that intermolecular specific interactions shifted to low wavenumber from 1709 cm^{-1} to 1707 cm^{-1}. When the content of *s*-PCL was set at 40 *wt*%, the opposite trend was observed and the evidence of crystallization (band at 1727 cm^{-1}) became clear. In other words, crystallization of the PCL subchains could not be restricted. The crystallization may be predominant, and affected by the crosslinking structure and intermolecular specific interactions. Although hydrogen bonding interactions still existed in the two amine-type cured systems, this kind of intermolecular force in DDS-cured systems was weaker than that in MOCA-cured systems [11]. This weak hydrogen bonding was insufficient to restrict PCL chains in the cured system, causing macroscopic phase separation. It was also affected by the PCL content in the mixtures [19–21].

3.4. Phase structure of epoxy thermosets

From the aforementioned analysis, it is clear that *s*-PCL was miscible with epoxy resin cured with MOCA. The intermolecular specific interactions also favored the miscibility between PCL subchains and epoxy matrix cured with DDS. However, the interactions did not suppress crystallization of *s*-PCL completely when the weight fraction of *s*-PCL was as high as 40 *wt*%. For epoxy thermosets containing *s*-PCL, the crosslinked networks inevitably retarded the chain folding of PCL and then restrain crystallization of PCL [16]. FESEM images of the epoxy thermosets containing *s*-PCL are shown in Fig. 5. It can be found that macro-phase separation did not occur for all the MOCA-cured epoxy thermosets (Fig. 5a–d). In consideration of the amphipathic nature of *s*-PCL in epoxy matrix, self-assembly behavior could occur. Hence, nanoscale dispersed phase could be observed. In Fig. 5a–d, dispersed phase with a diameter of dozens of nanometers can be observed in the MOCA-cured epoxy thermosets, especially for the epoxy thermoset with 40 *wt*% *s*-PCL. For this curing system, nanostructures were readily achieved even along with crystals due to strong intermolecular specific interactions [22]. In contrast, the epoxy thermosets cured by DDS

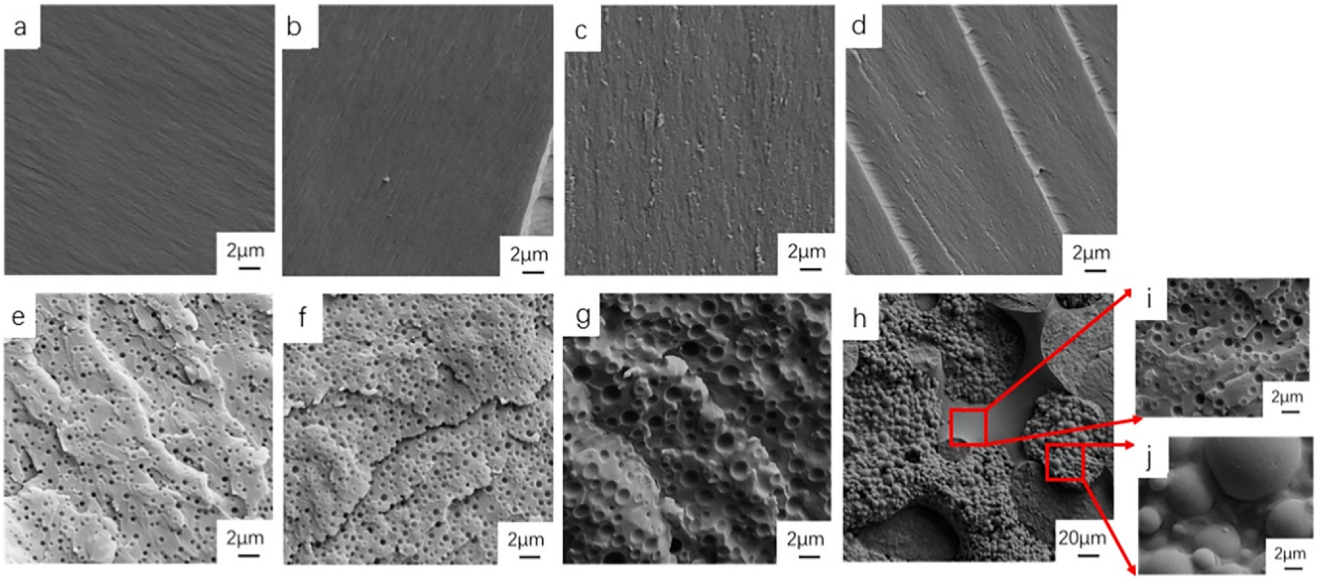

Fig. 5. FESEM images of the epoxy thermosets. (a)–(d) cured by MOCA, containing (a) 10, (b) 20, (c) 30 and (d) 40 *wt*% of *s*-PCL; (e)–(j) cured by DDS, containing (e) 10, (f) 20, (g) 30 and (h)–(j) 40 *wt*% of *s*-PCL.

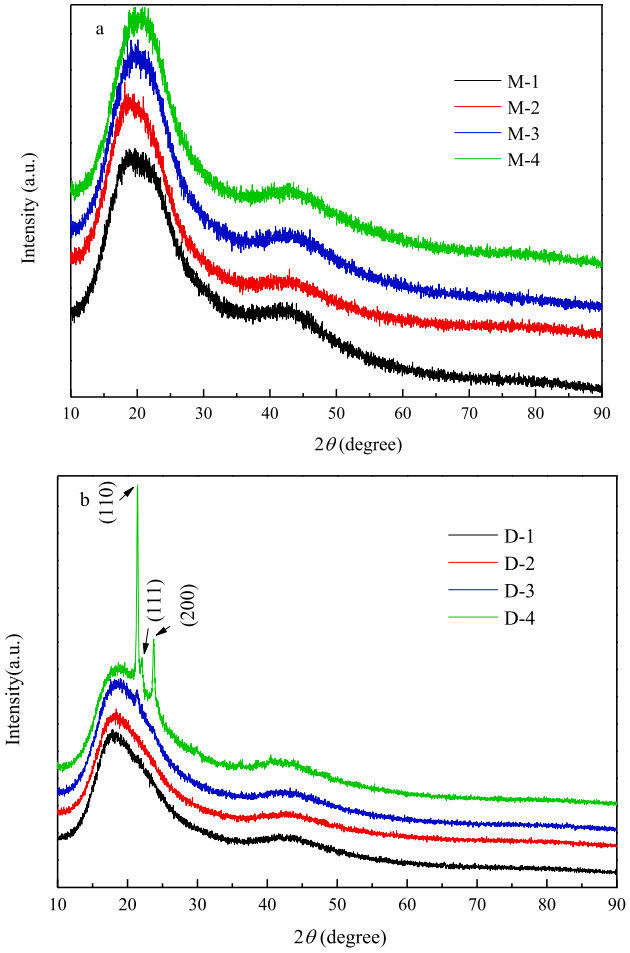

Fig. 6. XRD profile of the epoxy thermosets containing *s*-PCL. (a) cured by MOCA; (b) cured by DDS.

(Fig. 5e–j), exhibited distinct microstructures. Spherical particles with the average diameter of 0.34 μm and 0.44 μm (Table S1) were observed when the weight fraction of *s*-PCL was 10 *wt*% and 20 *wt*%, respectively. The diameter of dispersed phase reached 1.06 μm when the concentration of *s*-PCL was 30 *wt*%. Moreover, volume fraction of the dispersed phase increased obviously. It should be noted that spherulites were observed in the thermoset with the incorporation of 40 *wt*% *s*-PCL, indicating that crystallization of the PCL was developed. Since phase structure has a significant impact on the properties of polymer blends, another problem could be revealed -Whether the dispersed phase was amorphous or crystalline for the DDS-cured epoxy thermosets with lower *s*-PCL concentration. If dispersed phase is crystalline, the degree of crystallinity should also be determined. In general, polymer materials with dispersed regions that are crystalline or highly ordered can effectively resist penetration of small molecules such as water. As a result, the degradation of the polymer material would not be easily impaired. To answer this question, XRD analysis was implemented in the study of the phase structure further.

The XRD profiles of epoxy thermosets cured with different hardeners are presented in Fig. 6. For MOCA-cured thermosets (Fig. 6a), there were only broad diffused peaks on the XRD curves, which are typical amorphous diffraction peaks. This indicates that all PCL crystals were not detected. As a semi-crystalline polymer, XRD pattern of PCL always shows sharp crystalline diffraction peaks between 20° and 30° [23]. The absence of crystallinity of *s*-PCL can be interpreted in the facts of those: 1) due to the intermolecular hydrogen bonds, *s*-PCL was miscible with DGEBA before and after curing with MOCA. After curing, *s*-PCL acted as plasticizer of the epoxy thermosets, which resulted in the decrease in glass transition temperature [24,25], which was verified by the DMA curves; 2) crosslinking structure of epoxy resin (3-D confinement) suppressed the chain folding of *s*-PCL, and hence hindered the crystallization of *s*-PCL [14]. On the other hand, for the DDS-cured thermosets, the results were remarkably different (Fig. 6b). With 40 *wt* % of *s*-PCL, the DDS-cured thermoset displayed sharp diffraction peaks at the diffraction angles (2θ) of 21.4°, 22.1° and 23.8°, respectively, corresponding to the crystal planes (1 1 0), (1 1 1) and (2 0 0) of PCL. The crystallinity of *s*-PCL was also calculated by the following equation approximately, Eq. (1) :

$$X_C = \frac{\sum I_C}{\sum I_C + \sum I_a} \quad (1)$$

where X_C is the crystallinity, $\sum I_C$ is the integrated intensity of crystal diffraction peaks, and $\sum I_a$ is the integrated intensity of amorphous diffraction peaks. According to the results of calculation, when the content of *s*-PCL reached 40 *wt*% in DDS-cured epoxy resin, its crystallinity was about 9%, which is in accordance with the fact that spherulitic structure could be detected by FESEM (Fig. 5j, l). The different branched chain structures or molecular weights of PCL would have an important impact on its crystallization behaviors [26,27], and intermolecular hydrogen interactions would also limit these behaviors significantly. However, the crystallization of PCL could not be suppressed when the content of *s*-PCL was high enough. Besides, there was a weak crystalline peak at 21.4° in these materials with 30 *wt*% of *s*-PCL and the degree of crystallization was difficult to calculate due to the weak peak intensity. For the samples containing 10–20 *wt*% of *s*-PCL, there was no obvious crystallinity detected by XRD measurement. It can be concluded that crystallinity of PCL was effectively suppressed when the content of *s*-PCL was lower than 30 *wt*% for the DDS cured system.

3.5. Dynamic mechanical thermal analysis of epoxy resin

The different crystallization behavior was further confirmed by dynamical mechanical thermal analysis, as shown in Fig. 7. It was found that αtransition temperature decreased with the increase in content of *s*-PCL for the MOCA-cured system (Fig. 7a and Table 2). With temperatures over the melting temperature of PCL, the storage moduli decreased rapidly, especially for the epoxy thermoset containing 40 *wt* % of *s*-PCL. For the DDS-cured system (Fig. 7b), the storage modulus can be maintained at a much higher temperature compared with MOCA-cured system, except for the sample with 40 *wt*% of *s*-PCL. Compared to other samples in DDS-cured system, when the crosslinked sample had 40 *wt*% of *s*-PCL, the storage moduli showed a different trend, decreasing in two stages with the increase in temperature. Therefore, crystallization of PCL in blends did not have a reinforcing effect on storage modulus. Crosslinking density may play an important role in improving the storage modulus [28]. In this work, the crosslinking density is discussed based on the equation derived from the theory of rubber elastic [29,30] Eq. (2):

$$v_e = \frac{E}{6RT} \quad (2)$$

where v_e is the crosslinking density, and its unit is mol/m^3; R is the gas constant, its value is 8.314J mol^{-1} K^{-1}; T is the absolute temperature, its value is the Kelvin temperature of T_g plus 40 K; and E is the storage modulus of the rubber plateau region.

The crosslinking densities of the obtained epoxy thermosets are summarized in Table 2. The results of crosslinking density exhibited a downward trend with the increase in content of *s*-PCL, regardless of the curing agent used. The storage moduli of DDS-cured epoxy thermosets containing 10–20 *wt*% of *s*-PCL could not be easily lowered compared to the samples cured with MOCA, although their crosslinking densities were similar. As discussed above, the miscibility between *s*-PCL and epoxy matrix cured with DDS was lower compared to the counterparts cured with MOCA. Chain orientation derived from de-mixing effect

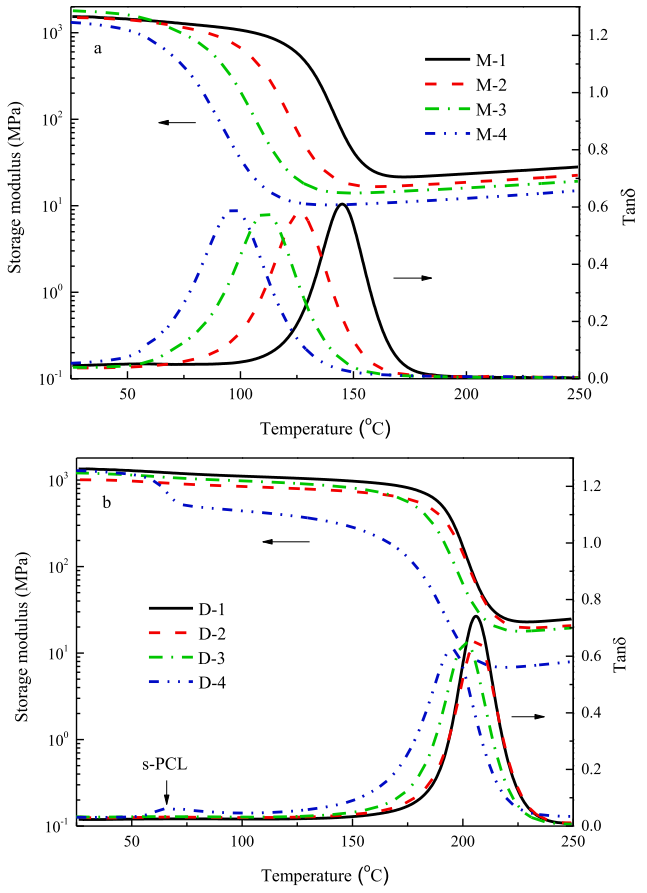

Fig. 7. DMA curves of the epoxy thermosets containing *s*-PCL. (a) cured by MOCA; (b) cured by DDS.

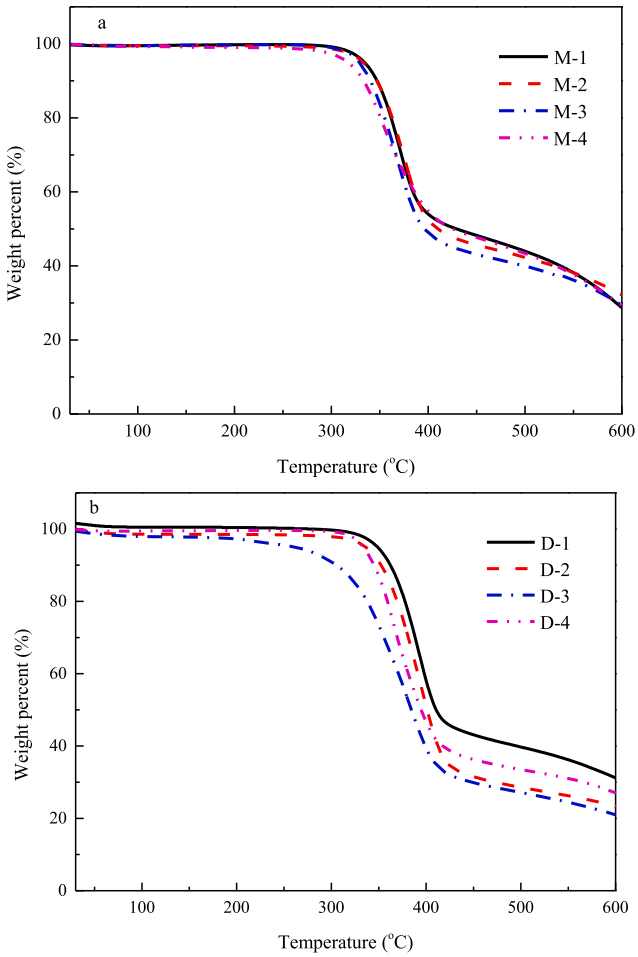

Fig. 8. TGA curves of the epoxy thermosets containing *s*-PCL. (a) cured by MOCA; (b) cured by DDS.

between the dispersed phase and the matrix should enhance storage modulus. However, there was an apparent decline when the heating temperature reached around 65 ˚C for the epoxy thermoset with 40 *wt*% of *s*-PCL. Moreover, there was a corresponding melting peak of *s*-PCL on the tanδ curve of this sample. Therefore, crystallization of *s*-PCL could not be completely suppressed despite the confinement of crosslinked networks. This is in good accordance with the results of XRD and FESEM. From the tanδ curves of DDS-cured samples, it was observed that the *α* transition temperature of epoxy thermosets shifted to lower temperatures with the increase in content of *s*-PCL. This result indicated that PCL was partially miscible with the epoxy matrix cured with DDS. The miscibility between linear PCL and epoxy thermosets cured with DDS has been investigated exhaustively previously [14]. Zheng proposed that the intermolecular specific interactions existing between carbonyl groups of linear PCL and hydroxyl groups of epoxy matrix were suppressed due to competitive hydrogen bonding interactions between OH···S═O and OH···C═O[11]. In this work, the *s*-PCL structure could enrich the local concentration of carbonyl groups in the same space reasonably. Thus, the association between carbonyl group and hydroxyl group of epoxy thermosets would be improved. This inference was supported by means of FTIR analysis above.

3.6. Thermal properties of epoxy thermosets

Change in structure has a significant impact on the properties of epoxy thermosets. Here, thermal gravimetric analysis (TGA) was used to analysis the thermal properties of the epoxy thermosets and these curves are illustrated in Fig. 8. Characteristic data are presented in Table 1. All the specimens exhibited two steps of thermal degradation behavior. The T_5 (the characteristic temperature corresponding to 5% weight loss) of MOCA-cured epoxy thermosets showed a slight reduction from 334 ˚C to 317 ˚C with the increase in content of *s*-PCL. In comparison, T_5 varied from 349 ˚C to 334 ˚C for the DDS-cured epoxy thermosets. Therefore, epoxy thermosets cured with DDS were more thermally stable than those cured with MOCA. Besides, thermal stability decreased with the increase in content of *s*-PCL. Interestingly, T_5 of the DDS-cured sample containing 40 *wt*% of *s*-PCL was 334 ˚C, obviously higher than other samples. Combined with the XRD analysis of the DDS-cured epoxy thermosets, *s*-PCL in these thermosets was almost amorphous when its' content was less than 40 *wt*%, yet there had a proportion of crystalline *s*-PCL in the thermoset containing 40 *wt*% *s*-

Table 2
Thermal dynamic mechanical properties of epoxy thermosets.

	M-1	M-2	M-3	M-4	D-1	D-2	D-3	D-4
T_g/˚C	145.00	126.30	111.10	97.00	205.90	206.40	201.20	195.10
T/K	458.15	439.45	424.25	410.15	519.05	519.55	514.35	508.25
E/MPa	22.19	16.76	14.02	10.23	24.37	20.59	18.82	7.32
$Ve/10^{-3}$ mol/cm^3	0.97	0.76	0.66	0.50	0.94	0.79	0.73	0.29

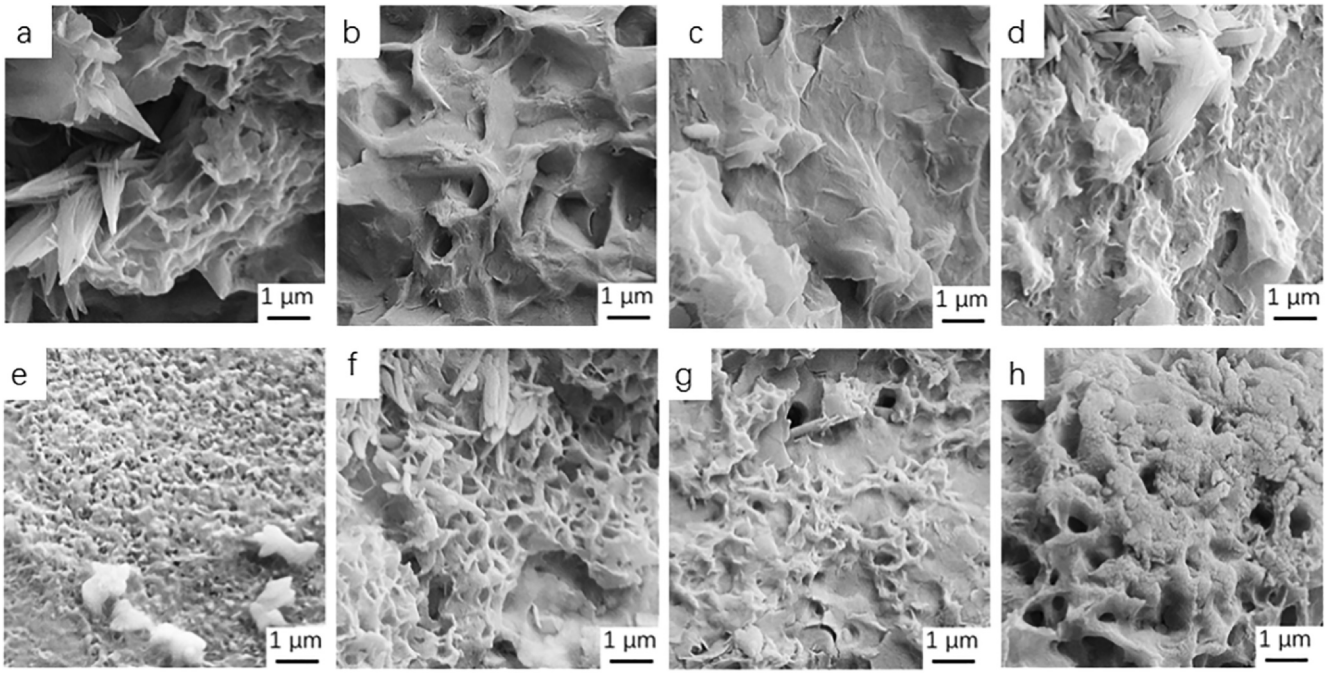

Fig. 9. FESEM images of the epoxy thermosets degraded in alkaline solution for 30 days. (a)–(d) cured by MOCA, (a) 10, (b) 20, (c) 30 and (d) 40 *wt*% of *s*-PCL; (e)–(h) cured by DDS, (e) 10, (f) 20, (g) 30 and (h) 40 *wt*% of *s*-PCL.

PCL. According to the relationship between the structure and properties of polymer, the condensed structure of the substance would affect the thermogravimetric behavior of polymers. Specifically, chain segments in crystalline part of *s*-PCL were stacked orderly, and their movements could consume more energy, for example, melting enthalpy, than that of amorphous *s*-PCL under heating, which led to an increase in the thermal decomposition temperature of these thermosets containing crystalline *s*-PCL. Besides, the crosslinking density and free volume content of epoxy resins may also affect their thermal stability [19,31,32].

3.7. Degradation of s-PCL/epoxy thermosets

Fig. 9 and Fig. S6 show the cross-sectional morphologies and photos of the two amine-type epoxy thermosets after being immersed in 10% NaOH aqueous solution for 30 days, respectively. It can be seen that holes and cracks were dispersed in the cross-sections of the epoxy matrixes. Before being immersed in NaOH aqueous solution, the surfaces of epoxy thermosets were relatively smooth, while irregular holes and many small cracks were observed after degradation and many fragments appeared in the solution. This is mainly because PCL was evenly distributed in the epoxy matrix, and a small amount of hydroxyl groups might tether to the end of PCL subchains participated in the reaction with the epoxy group. This reaction introduced a large number of ether bonds, which could provide active points of degradation, into the structures of epoxy thermosets. These ether bonds together with the ester groups of PCL would undergo cleavage under alkaline environment. In addition, epoxy resin could also absorb a certain amount of water to deteriorate PCL. Moreover, water absorption may locally generate internal stress in the epoxy matrixes [33–36]. When the internal stress is large enough, cracks would be produced, which could also promote the NaOH aqueous solution to penetrate into the interior gradually. In addition, the epoxy thermosets cured with MOCA were more sensitive to alkaline degradation than that cured by DDS. More holes and cracks were found in the MOCA-cured samples than the DDS-cured samples for the same *s*-PCL content. This was probably due to the difference in intermolecular specific interactions between *s*-PCL and the two epoxy matrixes. In particular, when the intermolecular specific interaction became weak and could no longer completely suppress the crystallization of PCL, degradation of PCL crystalline microdomains was observed on the surface of the epoxy thermoset containing 40 *wt*% *s*-PCL by FESEM. The PCL spherulites are hard to be attacked of alkaline solution for the same amount, because PCL subchains stacked closely and the solution was not easy to diffuse into spherulites. As depicted in Fig. 10, alkaline solution would attack the dispersed phase step by step if there are no PCL crystals in the matrix. Moreover, alkaline solution (viz. NaOH aqueous solution) would deteriorated the PCL spherulite to some degree, which was also detected in the film of tetra-armed PCL-*b*-PDLA diblock copolymer [37].

4. Conclusion

We synthesized the six-arm star PCL with cyclotriphosphazene core *via* ROP successfully, and then introduced into epoxy thermosets cured with MOCA and DDS, respectively. Intermolecular specific interactions affected the morphologies of the thermosets significantly. Due to the miscibility between *s*-PCL and epoxy thermosets, there was no macrophase separation for all the epoxy thermosets cured with MOCA. However, it was different for the DDS-cured system. The six-arm copolymer was partially miscible with the epoxy matrix cured with DDS, which might be due to the enriched local concentration of carbonyl groups in the hybrid copolymer. Consequently, amorphous dispersed phases with diameter of 0.34–0.44 μm were found in the epoxy thermosets cured with DDS containing 10–20 *wt*% *s*-PCL. However, crystallization of PCL was not completely suppressed when the content of *s*-PCL was more than 30 *wt*%, although the crystallization of PCL was hindered by intermolecular specific interactions and crosslinking networks of the epoxy thermosets. The difference in microphase structure in turn had an important influence on the thermal and alkaline degradation of the epoxy thermosets. Interestingly, the MOCA-cured and DDS-cured crosslinked blends were more resistant to thermal degradation but were more sensitive to alkaline degradation. MOCA-cured thermosets were degraded more easily by alkaline than DDS-cured thermosets. And we believe that this work may give the inspiration for design of a recycling path for thermosets after their service life.

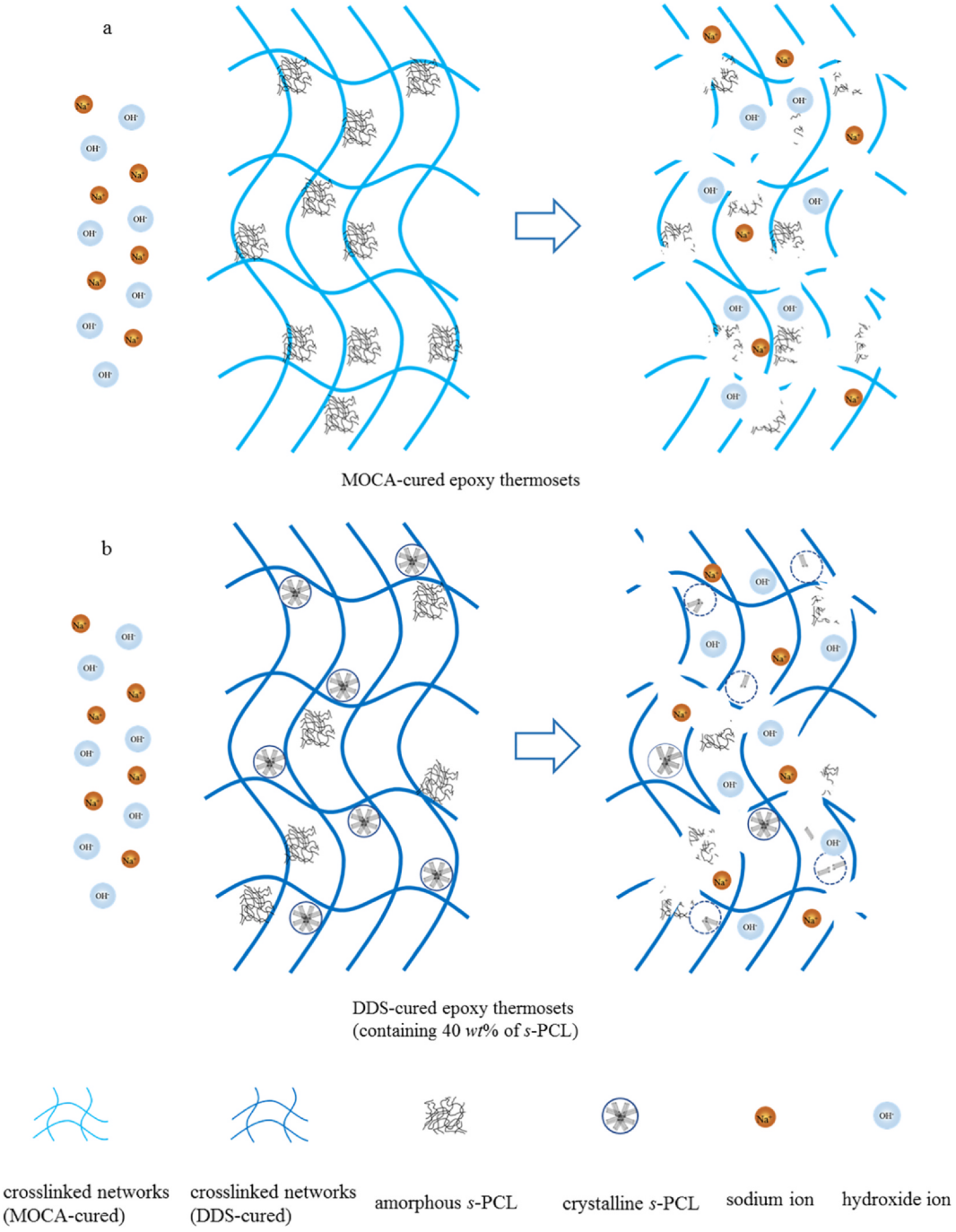

Fig. 10. Schematic diagram of epoxy thermosets degradation. (a) MOCA-cured epoxy thermosets; (b) DDS-cured epoxy thermosets containing 40 *wt*% of *s*-PCL.

CRediT authorship contribution statement

Pengli Zhang: Investigation, Validation, Formal analysis, Writing - original draft. **Yanfang Zhao:** Validation, Resources, Writing - review & editing. **Rentong Yu:** Conceptualization, Supervision, Resources, Writing - review & editing. **Jianhe Liao:** Funding acquisition, Supervision, Writing - review & editing.

Declaration of Competing Interest

The authors declare that they have no known competing financial interests or personal relationships that could have appeared to influence the work reported in this paper.

Acknowledgement

The authors are grateful to the Analytical and Testing Center of Hainan University for their help of analytical measurements. The financial support of the National Natural Science Foundation of China (Grant No. 51403045) is acknowledged.

Appendix A. Supplementary material

Supplementary data to this article can be found online at https://doi.org/10.1016/j.eurpolymj.2020.109989.

References

[1] P.M. Lipic, F.S. Bates, M.A. Meyers, Nanostructured thermosets from self-assembled amphiphilic block copolymer/epoxy resin mixtures, J. Am. Chem. Soc. 120 (35) (1998) 8963–8970.

[2] F. Meng, S. Zheng, H. Li, Q. Liang, T. Liu, Formation of ordered nanostructures in epoxy thermosets: A mechanism of reaction-induced microphase separation, Macromolecules 39 (15) (2006) 5072–5080.

[3] A.K. Sharma, R. Sloan, R. Ramakrishnan, S.I. Nazarenko, Structure-property relationships in epoxy hybrid networks based on high mass fraction pendant POSS incorporated at molecular level, Polymer 139 (14) (2018) 201–212.

[4] Q. Zhou, Q. Liu, N. Song, J. Yang, L. Ni, Amphiphilic reactive poly(glycidyl methacrylate)-block-poly(dimethyl siloxane)-block-poly(glycidyl methacrylate) triblock copolymer for the controlling nanodomain morphology of epoxy thermosets, Eur. Polym. J. 120 (2019) 109236.

[5] J. Liu, Z.J. Thompson, H.-J. Sue, F.S. Bates, M.A. Hillmyer, M. Dettloff, G. Jacob, N. Verghese, H. Pham, Toughening of epoxies with block copolymer micelles of wormlike morphology, Macromolecules 43 (17) (2010) 7238–7243.

[6] Y. Xiang, L. Li, S. Zheng, Morphologies and dielectric properties of epoxy thermoset containing poly(N-vinylcarbazole), fullerene-C_{60} and their charge transfer complex nonaphases, Polymer 138 (28) (2018) 113–123.

[7] X.B. Wang, T.-C. Lin, H.-Y. Hsueh, S.-C. Lin, X.-D. He, R.-M. Ho, Nanoporous gyroid-structured epoxy from block copolymer templates for high protein adsorbability, Langmuir 32 (25) (2016) 6419–6428.

[8] Y. Xiang, S. Xu, S. Zheng, Epoxy toughening via formation of polyisoprene nanophases with amphiphilic diblock copolymer, Eur. Polym. J. 98 (2018) 321–329.

[9] X.F. Sánchez-Romate, J. Martín, A. Jiménez-Suárez, S.G. Prolongo, AlejandroUreña, Mechanical and strain sensing properties of carbon nanotube reinforced epoxy/poly (caprolactone) blends, Polymer 190 (2020) 122236.

[10] J. Parameswaranpillai, M.R. Sanjay, S. Siengchin, S.K. Sidhardhan, N. Hameed, Intermolecular hydrogen bonding in developing nanostructured epoxy shape memory thermosets: Effects on morphology, thermo-mechanical properties and surface wetting, Polym. Test. 81 (2020) 106279.

[11] Y. Ni, S. Zheng, Influence of intramolecular specific interactions on phase behavior of epoxy resin and poly(ε-caprolactone) blends cured with aromatic amines, Polymer 46 (15) (2005) 5828–5839.

[12] Q. Guo, R. Thomann, W. Gronski, T. Thurn-Albrecht, Phase behavior, crystallization and hierarchical nanostructures in self-organized thermoset blends of epoxy resin and amphiphilic poly(ethylene oxide)-block-poly(propylene oxide)-block-poly (ethylene oxide) triblock copolymers, Macromolecules 35 (8) (2002) 3133–3144.

[13] W. Ye, W. Wei, X. Fei, R. Lu, N. Liu, Six-arm star-shaped polymer with cyclophosphazene core and poly(ε-caprolactone) arms as modifier of epoxy thermosets, J. Appl. Polym. Sci. 134 (2) (2017).

[14] P.M. Remiro, M.M. Cortazar, M.E. Calahorra, Miscibility and crystallization of an amine-cured epoxy resin modified with crystalline poly(ε-caprolactone), Macromol. Chem. Phys. 202 (7) (2001) 1077–1088.

[15] J. Parameswaranpillai, S.K. Sidhardhan, S. Jose, N. Hameed, N.V. Salim, S. Siengchin, J. Pionteck, A. Magueresse, Y. Grohens, Miscibility, phase morphology, thermo-mechanical, viscoelastic and surface properties of PCL modified epoxy systems: Effect of curing agents, Ind. Eng. Chem. Res. 55 (38) (2016) 10055–10064.

[16] H. Lv, Miscibility, phase behavior, specific intermolecular interaction in thermosetting polymer blends, School of Chemistry and Chemical Engineering, ShangHai JiaoTong University, 2003.

[17] W.-C. Su, F.-C. Tsai, C.-F. Huang, L. Dai, S.-W. Kuo, Flexible epoxy resins formed by blending with the diblock copolymer PEO-b-PCL and using a hydrogen-bonding benzoxazine as the curing agent, Polymers 11 (2) (2019) 201.

[18] Y. Cui, X. Ma, X. Tang, Y. Luo, Synthesis, characterization and thermal stability of star-shaped poly(ε-caprolactone) with phosphazene core, Eur. Polym. J. 40 (2) (2004) 299–305.

[19] X. Xiong, L. Zhou, R. Ren, S. Liu, P. Chen, The thermal decomposition behavior and kinetics of epoxy resins cured with a novel phthalide-containing aromatic diamine, Polymer Test. 68 (2018) 46–52.

[20] I.M. Kalogeras, A. Stathopoulos, A. Vassilikou-Dova, W. Brostow, Nanoscale confinement effects on the relaxation dynamics in networks of diglycidyl ether of bisphenol-A and low-molecular-weight poly(ethylene oxide), J. Phys. Chem. B 111 (11) (2007) 2774–2782.

[21] Q. Guo, R. Thomann, W. Gronski, R. Staneva, R. Ivanova, B. Stühn, Nanostructures, semicrytalline morphology, and nanoscale confinement effect on the crystallization kinetics in self-organized block copolymer/thermoset blends, Macromolecules 36 (10) (2003) 3635–3645.

[22] C. Zhang, L. Li, S. Zheng, Formation and confined crystallization of polyethylene nanophases in epoxy thermosets, Macromolecules 46 (7) (2013) 2740–2753.

[23] E.M. Abdelrazek, A.M. Hezma, A. El-khodary, A.M. Elzayat, Spectroscopic studies and thermal properties of PCL/PMMA biopolymer blend 3(1) (2019) 10–15.

[24] Z. Xu, S. Zheng, Morphology and thermomechanical properties of nanostructured thermosetting blends of epoxy resin and poly(ε-caprolactone)-block-poly-dimethylsiloxane-block-poly(ε-caprolactone) triblock copolymer, Polymer 48 (20) (2007) 6134–6144.

[25] Y. Yao, J. Wang, H. Lu, B. Xu, Y. Fu, Y. Liu, J. Leng, Thermosetting epoxy resin/thermoplastic system with combined shape memory and self-healing properties, Smart Mater. Struct. 25 (1) (2016) 015021.

[26] J.-L. Wang, L. Wang, C.-M. Dong, Synthesis, crystallization and morphology of star-shaped poly(ε-caprolactone), J. Polym. Sci., Part A: Polym. Chem. 43 (22) (2005) 5449–5457.

[27] M.J. Jenkins, K.L. Harrison, The effect of molecular weight on the crystallization kinetics of polycaprolactone, Polym. Adv. Technol. 17 (6) (2006) 474–478.

[28] M. Yohei, K. Junosuke, Y. Kohbara, K. Shoichi, Dynamic ionic crosslinks enable high strength and ultrastretchability in a single elastomer, Commun. Chem. 1 (1) (2018) 1–5.

[29] R. Hagen, L. Salmen, B. Stenberg, Effects of the type of crosslink on viscoelastic properties of natural rubber, J. Polym. Sci., Part B: Polym. Phys. 34 (1996) 1997–2006.

[30] X. Li, P. Zhang, J. Dong, F. Gan, X. Zhao, Q. Zhang, Preparation of low-κ polyimide resin with outstanding stability of dielectric properties versus temperature by adding a reactive Cardo-containing diluent, Compos. B Eng. 177 (15) (2019) 107401.

[31] Q. Yong, P. Wei, P. Jiang, X. Zhao, H. Yu, Synthesis of a novel hybrid synergistic flame retardant and its application in PP/IFR, Polym. Degrad. Stab. 96 (6) (2011) 1134–1140.

[32] G. You, Z. Cheng, H. Peng, H. He, Synthesis and performance of a novel nitrogen-containing cyclic phosphate for intumescent flame retardant and its application in epoxy resin, J. Appl. Polym. Sci. 132 (16) (2015) 41859.

[33] M.C. Lee, N.A. Peppas, Water transport in graphite/epoxy composites, J. Appl. Polym. Sci. 47 (8) (1993) 1349–1359.

[34] K. Bociong, A. Szczesio, K. Sokolowski, M. Domarecka, J. Sokolowski, M. Krasowski, M. Lukomska-Szymanska, The influence of water sorption of dental light-cured composites on shrinkage stress, Materials 10 (10) (2017) 1142.

[35] J.F. McCabe, S. Rusby, Water absorption, dimensional change and radial pressure in resin matrix dental restorative materials, Biomaterials 25 (18) (2004) 4001–4007.

[36] O. Starkova, S. Chandrasekaran, T. Schnoor, J. Sevcenko, K. Schulte, Anomalous water diffusion in epoxy/carbon nanoparticle composites, Polym. Degrad. Stab. 164 (2019) 127–135.

[37] Z. Ning, J. Ni, Z. Gan, Four-armed PCL-b-PDLA diblock copolymer: 1. Synthesis, crystallization and degradation, Polymer Degrad. Stabil. 107 (2014) 120–128.

Dr. Rentong Yu is focusing on polymer phase structure, polymer ultrafiltration membrane and natural rubber modification in Hainan University. He earned his PhD from Shanghai Jiaotong University. He has published papers in Macromolecules, polymer, Industrial & Engineering Chemistry Research, etc.